PERGAMON

International Journal of Multiphase Flow 25 (1999) 1601–1618

International Journal of Multiphase Flow

www.elsevier.com/locate/ijmulflow

Characteristics of film condensation of supersaturated steam–air mixture on a flat plate

Hie Chan Kang[a,*], Moo Hwan Kim[b]

[a]School of Mechanical Engineering, Kunsan National University, Kunsan, 573-701, South Korea
[b]Department of Mechanical Engineering, Pohang University of Science and Technology, Pohang, 790-784, South Korea

Received 28 March 1998; received in revised form 24 November 1998

Abstract

Experimental and numerical work was performed for the laminar film condensation of steam–air mixture flow over a flat plate. For small temperature difference between the gas mixture and the cold wall, the gas mixture in the boundary layer can be treated as superheated gas. When the temperature difference is large, the gas mixture becomes supersaturated near the interface. In that case, mist formed near the interface, the temperature profile of the gas mixture was greatly concaved toward the interface and the heat transfer was enhanced. However the velocity profile measured by the laser Doppler anemometer (LDA) showed the same trend without mist formation. A calculation model is proposed and compared with the experimental data and previous models for the superheated or the saturated conditions.

Keywords: Film condensation; Supersaturation; Gas-mixture; Stratified flow; Mist formation; Two-phase flow; Boundary layer; Heat transfer

1. Introduction

Film condensation is one of the most important factors in connection with heat exchangers and nuclear power plants. Film condensation in the containment building would be the last passive system to maintain safety in case of accidental coolant loss in a nuclear power plant.

A lot of studies on film condensation have been done for various modes after the work of Nusselt (1916). The modes are classified according to the flow regime of vapor, the status of

* Corresponding author. Tel.: +82-654-469-4722; fax: +82-654-466-2086.
E-mail address: hckang@ks.kunsan.ac.kr (H.C. Kang)

0301-9322/99/$ - see front matter
PII: S0301-9322(98)00077-9

condensing interface, the presence of non-condensable gas and, the orientation of condensing surface, etc.

In the presence of noncondensable gas, thermal resistance is classified into the thermal resistance of condensate film and the mixture boundary layer as shown in Fig. 1. The presence of noncondensable gas greatly reduces the heat transfer in the condensation process (Sparrow and Gregg, 1959; Minkowycz and Sparrow, 1966; Sparrow et al., 1967; Rauscher et al., 1974; and Asano et al., 1979). Corradini (1984), Chen et al. (1987), and Kim and Corradini (1990) solved the condensation heat transfer problem by using the heat and mass transfer. Denny et al. (1971) conducted a numerical simulation for the film condensation of steam–air mixture flowing over a vertical surface. Jones and Renz (1974) calculated the turbulence boundary layer of CCl_4–air mixture by using the k–ϵ model. Desesquelles and Foch (1986) conducted experiments and numerical simulations for steam–air mixture flow over the flat plate. These works were done assuming the mixture without mist generation or superheated condition.

The expansion of steam in a nozzle is an example of a process in which supersaturation of vapor may occur (Wylen and Sonntag, 1976). Experimentally, condensation is almost never found to occur exactly at the point of the saturated vapor curve, where it should occur if thermodynamic equilibrium existed. Instead, condensation is observed to occur abruptly in what is usually called condensation shock. Vapor that is supersaturated above its equilibrium saturation pressure exists in a non-equilibrium condition referred to as a metastable state. Supersaturation was studied and summarized by Gyarmathy (1963), Hill (1966), Wegener and Wu (1977) and Carey (1992). The supersaturation limit is defined as critical pressure ($P_{G,ssl}$) forming droplets at the supersaturated condition. The net flux of the number of droplet embryos in the size space, J, is:

$$J = \sqrt{\frac{2}{\pi}} \frac{N_A^{2/3}}{R} \left(\frac{P_G}{T}\right)^2 \frac{\sqrt{\sigma_L M_G}}{\rho_L} \exp\left[-\frac{n^* \ln(P_G/P)}{2}\right] \tag{1}$$

where N_A, R, P_G, T, σ_L, ρ_L and M_G are the Avogadro's number, the gas constant of vapor,

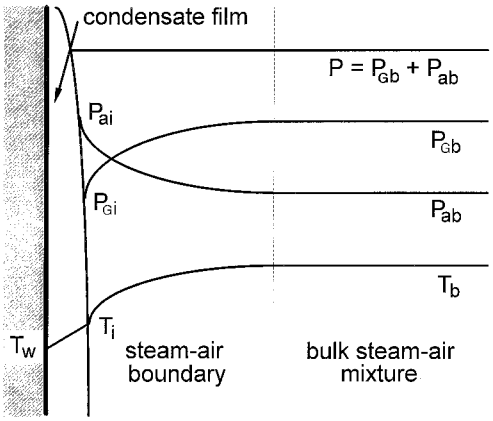

Fig. 1. The boundary layers in the presence of noncondensable gas on film condensation.

the vapor pressure, the temperature, the surface tension of liquid, the density of liquid and the molecular weight of vapor, respectively. And the number of molecules in a cluster 'n^*' and the critical radius of droplet 'r^*' are expressed as below:

$$n^* = (4\pi/3)\rho_L(N_A/M_G)(r^*)^3$$

$$r^* = \frac{(2\sigma_L M_G)}{RT\rho_L \ \ln(P_G/P)} \tag{2}$$

Carey (1992) suggested $J = 10^6$ m^{-3} s^{-1} as the supersaturation limits for droplet nucleation. The limit of supersaturation ($\rho_{G,ssl}/\rho$) is shown in Fig. 2 as the dashed line. The solid line shows the saturation curve; it was obtained by the following equation:

$$W_{G,sat} = \frac{\rho_{G,sat}}{\rho} = \frac{(P_{sat}/P)(M_G/M_a)}{1-(P_{sat}/P)(1-M_G/M_a)} \tag{3}$$

where W is the mass concentration and, the subscripts G, a, L and sat mean the vapor, the air, the liquid or water and the saturation conditions, respectively.

If the mixture in the free stream is saturated and the interface is saturated, then the boundary layer will be supersaturated (left-hand side of solid line in Fig. 2). There is a possibility that mist or fog will spontaneously generate. In this phase changing process, the latent heat will increase the mixture temperature. The mist formation in the boundary layer

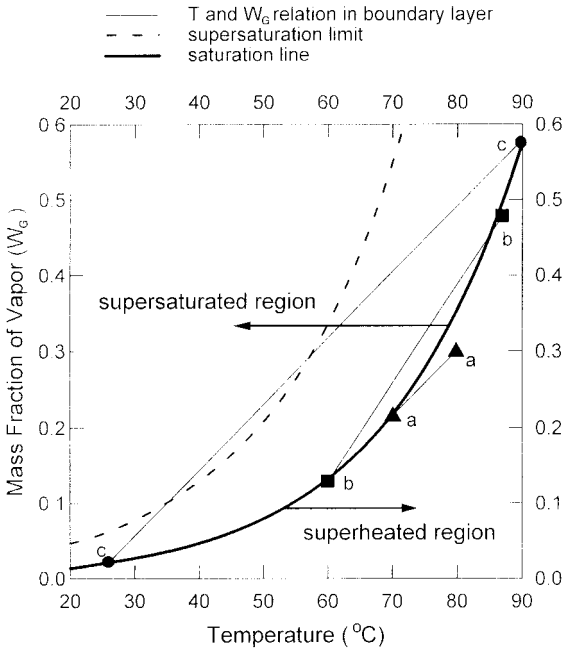

Fig. 2. Saturation curve and supersaturation limit of steam–air mixture and relation between temperature and steam mass fraction in the boundary layer.

was studied by Mori and Hijikata (1973), Brouwers (1991), Brouwers and Chesters (1992) and Fox et al. (1993). However there is no verification of their results with experimental data. Also it is very hard to find experimental data on the boundary layer of a supersaturated mixture.

The present work was performed for the film condensation of steam–air mixture over a flat plate having a smooth condensing interface. We focused on the characteristics of the supersaturated steam–air mixture on the momentum, heat and mass transfer. The present work provides experimental data for the velocity and thermal boundary layers. We applied superheated and equilibrium models and suggested a model to predict the condensation heat transfer of the supersaturated mixture.

2. Experimental method

2.1. Experimental facility

The present experimental facility consisted of main test section and auxiliary equipment: a steam generator, an air blower, an air preheater, a secondary condenser and water film control system. The main test section, as shown in Fig. 3, consisted of a cold block, a cooling channel, a rectangular cover and water injection/drain chambers. The cross sectional view of the main test section is shown in Fig. 4. The rectangular cover was made from 12.7 mm thick, transparent polycarbonate plates. The dimensions were 98.4 mm in height, 150 mm in width and 1720 mm in length. The duct was declined at 4.1° from the horizontal to investigate the various shapes of wavy interface. An aluminum block was used as the cold plate on which the condensate film was formed, and its dimensions were 25 mm in thickness, 150 mm in width and 1520 mm in length. It was cooled on the bottom side by running water. The role of the block was to maintain a constant temperature and to measure the heat flux.

The steam flow was provided by an electric boiler that has the capacity to produce 106 kg/h of saturated steam at atmospheric pressure. The steam produced from the steam generator was introduced to the mixing chamber through 47.1 mm i.d. stainless steel pipe. The operating

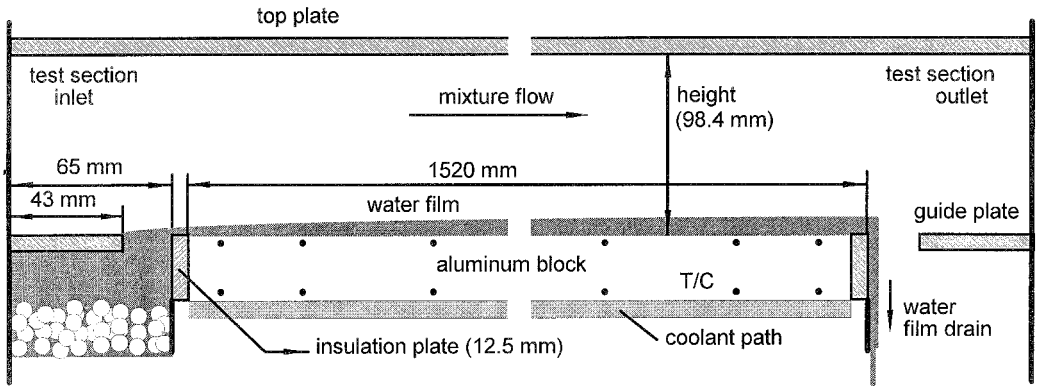

Fig. 3. Schematic diagram of main test section used in the present work.

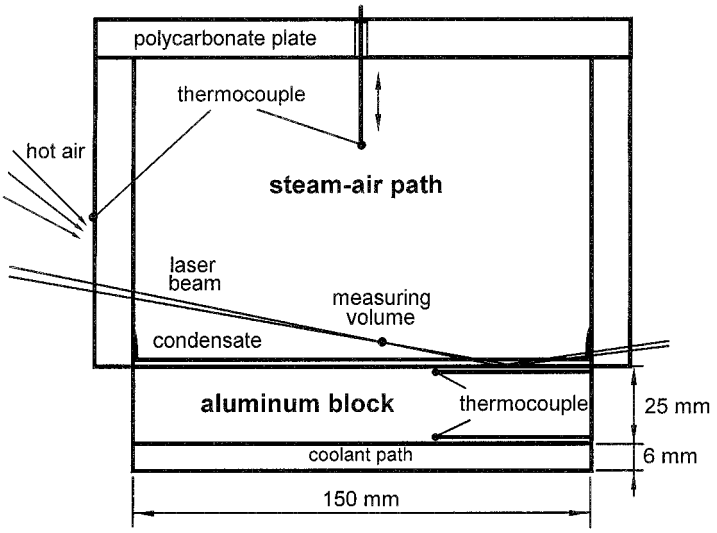

Fig. 4. Cross sectional view of main test section, laser trajectory to measure the mixture velocity, and thermocouples to measure the mixture temperature and heat flux.

pressure of the steam generator was about 20 kPa gauge pressure. The pressure compensated for the pressure loss in the pipe line and orifice, the exit temperature of the steam line was 100.4 ± 0.4°C. The air flow was provided by a 1.5 kW air blower, whose capacity was about 0.25 m^3/s at about 1.5 kPa gauge pressure. A variable-speed motor controller adjusted the flow rate. To obtain a saturated condition of the gas mixture, the air was heated before mixing with the steam by the air preheater, with about 7 kW full power. The chamber to refine the gas mixture flow was located between the air/steam mixer and the test section inlet. It consisted of a honeycomb, two screens and a settling chamber. All surfaces of the steam and air paths were insulated by 25 mm thick glass wool to reduce heat loss and unnecessary condensation in the test facility during the steady-state operation. The water was not injected at the inlet of test section in the present experiment. The condensed water was spontaneously formed on the aluminum block and drained at the end of test duct.

The purpose of the secondary condenser was to condensate the remaining steam that passed through the test section. The drained water from the cooling channel of the test section was reused as the coolant for the secondary condenser. The test conditions of the present experiment are listed in Table 1. The detail of the experimental setup is described in Kang and Kim (1994).

2.2. Measurement

The steam and air flow rates were measured by D and D/2 type orifice flow meters designed according to the British standard (1964). The diameter ratios were changed from 0.18 to 0.51 for the air orifice and from 0.23 to 0.32 for the steam orifice to measure a wide range of flow rates. The pressure drops between the orifice plates were measured by two pressure

Table 1
Test conditions of the present work

Items	Condition
Gas mixture	Steam–air mixture
Pressure	Ambient pressure
Velocity of gas mixture[a]	Less than 2 m/s
Reynolds number	$< 1.5 \times 10^5$
Temperature of gas mixture[a]	70–90°C
Air mass fraction of gas mixture[a]	0.42–0.78
Wall temperature	20–40°C
State[a]	Saturated
Declination angle	4.1° and 90°

[a] Properties measured at the inlet of test section.

transducers, Kyowa-PD100GA and Furness-FCO-012 for air and steam, respectively. The volume flow rate was checked by integration of the velocity profile of gases in the test section inlet, and the error was less than 5%. A digital-controller composed of IBM AT and DC motor driven gate valve was installed to obtain a steady steam flow rate.

The temperatures were measured at the steam inlet, the gas mixture inlet and the coolant inlet and exit by using 0.25 mm diameter T-type thermocouples. Thirty-two T-type thermocouples were installed around the boundary of the aluminum block to estimate the local heat flow rate as shown in Figs. 3 and 4. The thermocouples were inserted 2 mm diameter and 50 mm long copper tubes, and the tubes were inserted into drilled holes of the same size. Gaps between the hole and copper tube were filled with solder. Thermocouples to measure the top and bottom wall temperatures were located 2.1 mm away from each surface.

The thermal conductivity was precisely measured by ULYAC, TC-7000 HNC thermal conductivity meter. Its value was 118.3 W/m°C at 28°C. A steady-state condition was obtained after 30 min operation. Two-dimensional heat transfer in the aluminum block was assumed. Using the measured heat flux, q_x, the local heat transfer coefficient, h_x, is obtained as follows:

$$h_x = \frac{q_x}{T_\infty - T_{w,x}} \tag{4}$$

where T_∞ and $T_{w,x}$ are the temperature of mixture in the free stream and the wall temperature.

The temperature profile was measured by 0.125 mm T-type thermocouple at 1.21 m downstream from the inlet. The thermocouple was inserted through 1.5 mm i.d. of stainless steel tube, and the tip was stopped up with waterproof epoxy. The tube was inserted into the hole on the top plate of the rectangular channel as shown in Fig. 4, and attached to the translation guide (Micro Control, MR-40) with 0.01 mm resolution. The temperature profiles were measured four times at each point, and the results were averaged.

The velocity of steam–air mixture is not easy to measure by any anemometer. The present work used the laser Doppler anemometer (DANTEC, 2D LDA). The LDA measurement was confirmed with the Pitot tube measurement. The suitability of the flow refiner and test duct was checked by the air velocity profile. The mean velocity profiles in the test duct agreed with

the one-seventh-power law. Moisture droplets among the steam–air mixture generated good burst signals for the frequency counter in the measurement of mixture velocity. In the practical operation, the laser beams were blocked by the condensate formed on the inside of test duct. The hot air was blown on the outer surface to remove the condensate as shown in Fig. 4. The incident beams were tilted about 4° from the horizon, since the condensate was not completely removed near the cold plate. About 500 burst signals were taken to measure the mixture velocity at each point. The velocity profile was obtained from the average of four to six measurements.

3. Analysis model

3.1. Governing equations and boundary conditions

The geometry and condition for the analysis model is the same as the experimental conditions discussed in the previous section, and they were assumed as shown in Fig. 5. In this analysis, we assumed the following:

1. The steam–air mixture and condensate are laminar and two-dimensional flow.
2. The velocity, temperature and concentration of the steam–air mixture at the inlet are uniform.
3. The radiation heat transfer and the viscous dissipation are negligible.
4. The velocity, thermal and concentration boundary layers are formed over the cold wall (the bottom aluminum plate) and the velocity boundary layer is only formed along the top wall, since the top wall is insulated.
5. The rate of condensation is governed by the ordinary molecular diffusion, the thermal diffusion is negligible (Kroger and Rohsenow, 1968).

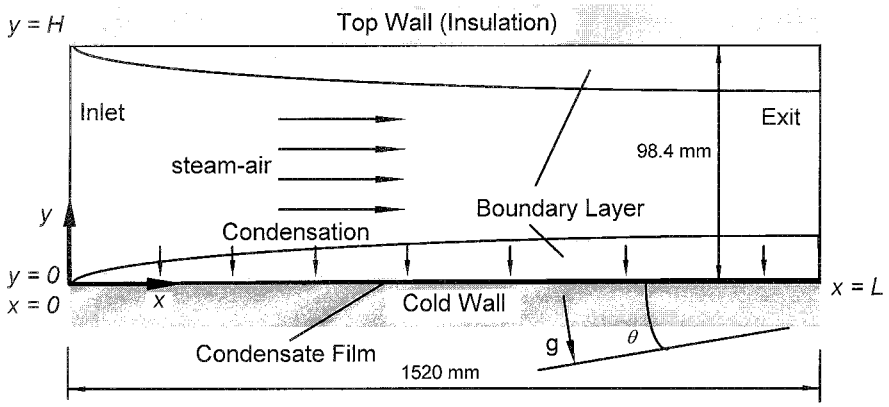

Fig. 5. Test geometry and coordinate systems for numerical calculation.

6. The mist formed in the steam–air mixture has negligible volume fraction compared with the gas mixture and it has a zero slip velocity relative to the mass average velocity as well as no diffusive component.
7. The condensate film formed on the cold surface is very thin, and the flow is laminar.
8. The convection heat transfer in the condensate film is negligible.

The continuity, the momentum, the energy, the air mass, the mist mass and the mist energy conservation equations are as below:

$$\frac{\partial \rho u}{\partial x} + \frac{\partial \rho v}{\partial y} = 0 \tag{5}$$

$$\frac{\partial \rho uu}{\partial x} + \frac{\partial \rho uv}{\partial y} = -\frac{\partial P}{\partial x} + \frac{\partial}{\partial x}\left(\mu \frac{\partial u}{\partial x}\right) + \frac{\partial}{\partial y}\left(\mu \frac{\partial u}{\partial y}\right) \tag{6}$$

$$\frac{\partial \rho u^2}{\partial x} + \frac{\partial \rho uv}{\partial y} = -\frac{\partial p}{\partial x} + \frac{\partial}{\partial x}\left(\mu \frac{\partial u}{\partial x}\right) + \frac{\partial}{\partial y}\left(\mu \frac{\partial u}{\partial y}\right) + g \sin \theta(\rho - \rho_r) \tag{7}$$

$$\frac{\partial \rho h' u}{\partial x} + \frac{\partial \rho h' v}{\partial y} = \frac{\partial}{\partial x}\left(k \frac{\partial T}{\partial x}\right) + \frac{\partial}{\partial y}\left(k \frac{\partial T}{\partial y}\right) \tag{8}$$

$$\frac{\partial \rho h' u}{\partial x} + \frac{\partial \rho h' v}{\partial y} = \frac{\partial}{\partial x}\left(k \frac{\partial T}{\partial x}\right) + \frac{\partial}{\partial y}\left(k \frac{\partial T}{\partial y}\right) \tag{9}$$

$$\frac{\partial \rho_L u}{\partial x} + \frac{\partial \rho_L v}{\partial y} = \dot{\rho}_L \tag{10}$$

$$\frac{\partial \rho_L u h_L}{\partial x} + \frac{\partial \rho_L v h_L}{\partial y} = \dot{q}_L \tag{11}$$

where μ, k and D are the dynamic viscosity, the thermal conductivity and the mass diffusivity of the mixture. The axis and velocity components are denoted in Fig. 5.

$$\rho = \rho_a + \rho_G + \rho_L \tag{12a}$$

$$\rho h' u = \rho_a h_a u_a + \rho_G h_G u_G + \rho_L h_L u_L \tag{12b}$$

$$\rho h' v = \rho_a h_a v_a + \rho_G h_G v_G + \rho_L h_L v_L \tag{12c}$$

$$h_a = c_{pa}(T - T_0) \tag{12d}$$

$$h_L = c_{pL}(T - T_0) \tag{12e}$$

$$h_G = c_{pG}(T - T_0) + h_{fg} \tag{12f}$$

The h, h_{fg}, c_p, T_0 are the enthalpy, the latent heat of vapor, the heat capacity and the reference temperature, respectively.

The insulation boundary conditions are applied for the top wall. The parabolic condition was used at the exit. The mass flux across the interface was obtained as below:

$$\text{at } y = \delta, \quad m_x = m_{x,G} + m_{x,L} = -(\rho_a + \rho_G)D\frac{\partial}{\partial y}\left(\frac{\rho_G}{\rho_a + \rho_G}\right) + \rho_L v_i \tag{13}$$

The boundary conditions for the interface are as below:

$$\delta = \left(\frac{3\mu_L \Gamma}{g \sin\theta \rho_L^2}\right)^{1/3}, \quad \Gamma = -\int_{x=0}^{x=x} m_x \, dx \tag{14}$$

$$\text{at } y = \delta, \quad v_i = \frac{\rho_a + \rho_G}{\rho_a}\left[D\frac{\partial}{\partial y}\left(\frac{\rho_a}{\rho_a + \rho_G}\right)\right]_i \tag{15a}$$

$$T_i = T_w - \left(h_G m_{x,G} + h_L m_{x,G} - k\left(\frac{\partial T}{\partial y}\right)_i\right)\frac{\delta}{k_L} \tag{15b}$$

$$\rho_G = \rho(W_{G,sat}) \tag{15c}$$

$$\frac{\partial \rho_L}{\partial y} = 0 \tag{15d}$$

$$\frac{\partial h_L}{\partial y} = 0 \tag{15e}$$

The δ, θ, Γ and the subscript i are the film thickness, the declination angle of the aluminum block, the condensate flow rate per unit width and the interface, respectively. The total heat flux across the interface is considered as the heat transfer by the vapor, the mist and the gas mixture as shown in the Eq. (15b).

3.2. Mist formation models

If the vapor pressure of superheated gas mixture is less or equal than the saturated pressure at a given temperature, then the gas mixture is superheated. Mist generation, $\dot{\rho}_L$ is zero as following equation.

$$P_G \le P_{sat}, \quad \dot{\rho}_L = 0 \tag{16}$$

We have tested three kinds of model for the supersaturated gas mixture ($P_G > P_{sat}$).

(a) *Superheated model*: this model assumes that there is no vapor formation in the gas mixture even though there is some disturbance, since the degree of supersaturation is small.

$$P_G > P_{sat}, \quad \dot{\rho}_L = 0 \tag{17}$$

(b) *Equilibrium model*: Hijikata and Mori (1973), Brouwers and Chesters (1992) and Fox et al. (1993) assumed that there would be some amount of vapor changed to the mist as the gas mixture reaches equilibrium if the mixture is supersaturated. In the process of phase change, the latent heat increases the mixture temperature. This model is written as below:

$$P_G > P_{sat}, \quad \Delta W_L = W_G^* - W_{G,sat} = \frac{c_p}{h_{fg}}(T - T^*) \tag{18}$$

The ΔW_L, W_G^*, $W_{G,sat}$, c_p, h_{fg}, T^*, and T_{sat} are the generated mist concentration, the initial mass concentration of vapor, the mass concentration of vapor at saturated condition, the heat capacity of mixture, the latent heat and the initial and the saturated temperatures, respectively.

(c) *Present model*: the present model proposes that the latent heat from the supersaturated mixture to saturated mixture be absorbed in the gas mixture. The β time of latent heat is accumulated in the mist as follows:

$$P_G > P_{sat}, \quad \Delta W_L = (W_G^* - W_{G,sat})(1 + \beta) \tag{19}$$

where

$$c_p(T - T^*) = h_{fg}\Delta W_L, \quad W_L(h_L - h_L^*) = \beta h_{fg}\Delta W_L \tag{20}$$

We used the β value as the supersaturation ratio P_{ssl}/P_{sat}. The β value ranged from 2.4 to 2.6 in the present test condition. In Eqs. (18) and (19), the final value $W_{G,sat}$ was obtained by using a Newton–Raphson root finding method.

3.3. Numerical simulation

The governing equations were solved by the finite difference method. We used the SIMPLER algorithm of Patanker (1980). The Cartesian coordinate and non-uniform grid was used to get fine grid spacing at the edge of the inlet and near the interface. A staggered grid was used, and the total number was 51 by 51 along x and y coordinates. The properties of steam–air mixture were calculated from the properties of saturated steam and air by using the averaged model of Reid et al. (1986). The calculation procedures are as below:

1. Using the properties of steam–air mixture, the velocity and temperature fields were solved. In this step, the interface was assumed to be a solid wall.
2. Using the fixed wall temperature condition, the mass concentration field of air was solved.
3. The interfacial temperature was obtained by using Eqs. (13)–(15c), and the velocity, temperature and concentration fields were calculated.
4. The mist generation conditions were applied for each control volume.

The conversion criteria were 10^{-5} for the residuals of mass and momentum equations and 10^{-3} for the changed values of all variables at each iteration, respectively. The suitability of the

present calculation was confirmed with the velocity profiles of Blasius for the laminar boundary layer over a flat plate.

4. Results and discussion

4.1. Film condensation of the superheated mixture

We tested the superheated steam–air mixture when the temperature of the gas mixture was higher than the saturated temperature or slightly less than the saturated mixture. The line a–a in Fig. 2 displays this condition. For line b–b in Fig. 2, the inlet, interface and free stream conditions are saturated. The mixture in the boundary layer may be supersaturated. However the degree of supersaturation is not much. The possibility of mist formation is not strong. We calculated the temperature profiles in the boundary layer having the same conditions of the experiment of Desesquelles and Foch (1986). They tested for the saturated steam–air mixture at the condition of the inlet temperature, $T_{in} = 80°C$, the inlet velocity, $u_{in} = 3$ m/s, the cold wall temperature, $T_w = 70.1°C$. The present and their numerical results are compared with their experimental data as shown in Fig. 6. The present results agree well with their measurement and calculation.

Fig. 7 shows the normalized velocity, temperature, and vapor mass fraction profiles by the interface and free stream values. The thick line shows the flow directional velocity profile without condensation. As shown in this figure, the boundary layer thickness is reduced due to

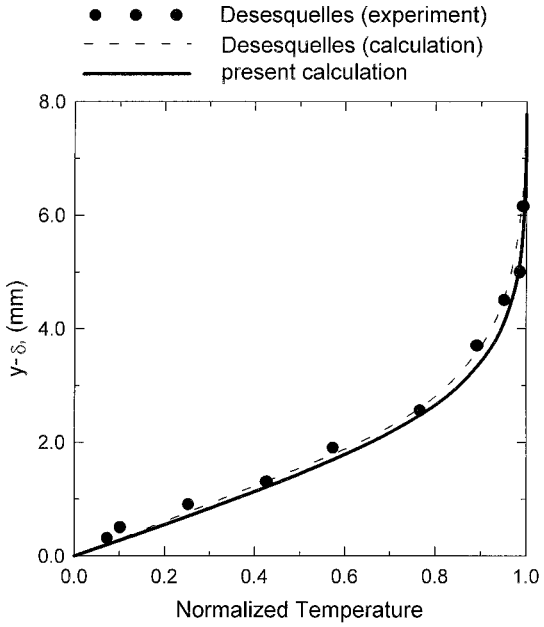

Fig. 6. Comparison of the temperature profile of the present calculation with the results of Desesquelles and Foch (1986) for the steam–air mixture. ($T_w = 70.1°C$, $T_{in} = 80°C$, $u_{in} = 3$ m/s at $x = 0.15$ m).

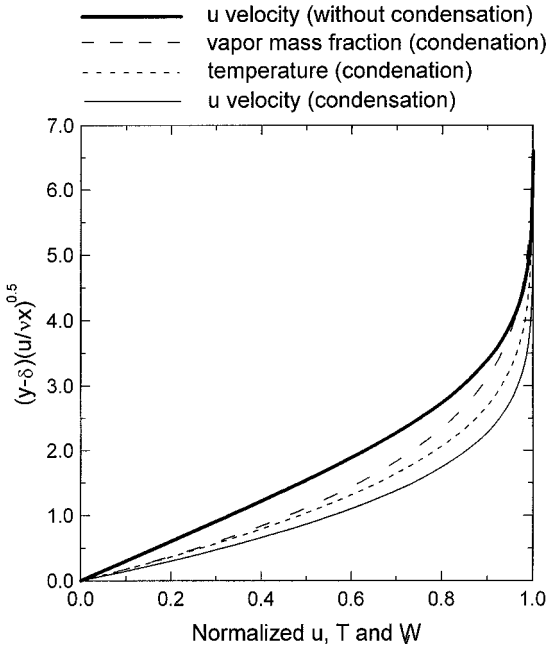

Fig. 7. Velocity, temperature and, mass concentration profiles of steam–air mixture with condensation and velocity profile without condensation. ($T_w = 80°C$, $T_{in} = 90°C$, $u_{in} = 2$ m/s at $x = 1.21$ m, $\theta = 4.1°$).

condensation. The reason for this is due to the mass diffusion of steam according to steam condensation. The thicknesses of thermal and concentration boundary layers are greater than that of velocity, because of the properties of mixture, the Prandtl number, $Pr = \nu/\alpha = 0.84$ and the Schmidt number, $Sc = \nu/D = 0.56$.

Fig. 8 compares the average heat transfer coefficient with the calculation and the measurement in the present work. The inlet mixture was saturated, and the temperature difference between the inlet and the wall was not much. The degree of supersaturation was small. The present calculation agrees well with the experimental data. From these results, we can conclude that the superheated or slightly supersaturated gas mixture can be treated as superheated gas mixture. We can say that the present calculations and experimental method are reliable.

4.2. Film condensation of supersaturated mixture

4.2.1. Superheated model

Fig. 9 shows the velocity and temperature profile in the boundary layer of supersaturated gas. The vertical axis of this figure was the distance measured from the interface. This case was tested for the conditions of $T_{in} = 90°C$, $T_w = 23.7°C$, $u_{in} = 2$ m/s, $\theta = 4.1°$. The temperature and velocity profiles were measured by the 0.25 mm T-type thermocouple and the DANTECH 2D LDA at 1.21 m from inlet. The normalized temperature profile is concaved toward the interface than the velocity profile. We applied the superheated model for this condition. The

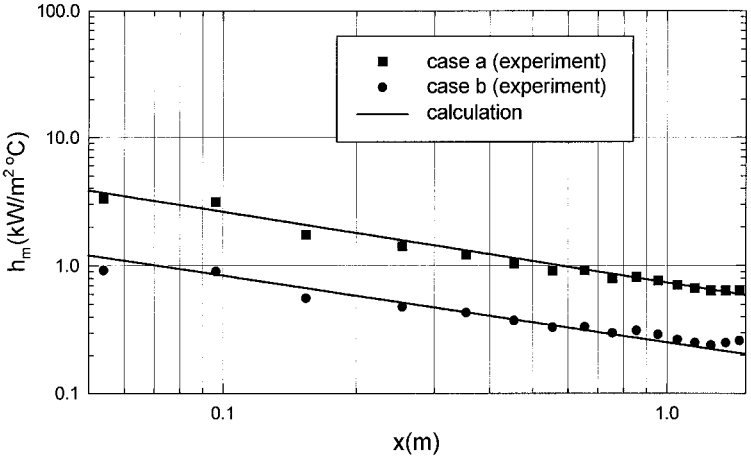

Fig. 8. Comparison of the numerical calculation with the experimental data for condensation heat transfer coefficient of saturated vapor (case a: $T_w = 67.2x^{-0.0483}$°C (x unit in m), $T_{in} = 95.9$°C, $u_{in} = 1.4$ m/s, $\theta = 87°$; case b: $T_w = 57.2\ x^{-0.0221}$°C (x unit in m), $T_{in} = 86.9$°C, $u_{in} = 1.4$ m/s, $\theta = 87°$).

calculated velocity profile (solid line) agrees well with the measured data (solid circle) by LDA. However, the temperature profile obtained by the numerical simulation using the superheated model is not similar to the experimental data. The flow regime can be assumed to be laminar flow. The velocity profile shows a similar trend to those of Figs. 6 and 7 calculated using the superheated model. The local Reynolds number ($Re_x = u_{in}x/\nu$) was 1.3×10^5. This value is far

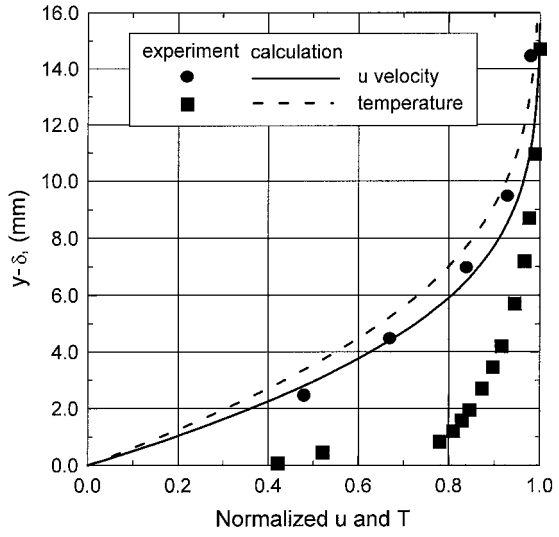

Fig. 9. Comparison of superheat model and experiment for the temperature and velocity profiles of steam–air mixture having large temperature difference between bulk mixture and wall ($T_w = 23.7$°C, $T_{in} = 90$°C, $u_{in} = 2$ m/s, $\theta = 4.1°$, $x = 1.21$ m).

less than the representative critical Reynolds number for a single-phase flow over a flat plate, $Re_{cr} = 5 \times 10^5$. The Re_{cr} might be a higher value in the present condition, since the condensation stabilizes the flow in the boundary layer. This test condition corresponds to the c–c line in Fig. 2. The whole boundary layer is located on the supersaturated region. Fig. 10 shows the comparison of the supersaturated model and the experimental data for the local heat transfer coefficient. The experimental data show 53% higher value than the results of the superheated model at $x = 1.0$ m. From these results, the superheated model predicted the velocity profile reasonably, however not the temperature and heat transfer.

4.2.2. Equilibrium model

The equilibrium model was applied to the two cases as shown in Figs. 11 and 12. The first is $T_{in} = 70°C$, $T_w = 18.5°C$, $u_{in} = 2$ m/s, $\theta = 4.1°$, $x = 1.21$ m. The other is $T_{in} = 90°C$, $T_w = 23.7°C$, $u_{in} = 2$ m/s, $\theta = 4.1°$, $x = 1.21$ m. The inlet condition was saturated for both cases. Hijikata and Mori (1973) and Brouwers (1991) and Brouwers and Chesters (1992) assumed that the supersaturated mixture in the boundary layer become the equilibrium condition ($T = T_{sat}$). The temperature profiles (dashed lines) obtained by using this model are closer to the experimental data than the superheated model. However the profiles near $y - \delta = 2$ mm were different. The heat transfer coefficient calculated by the equilibrium model is about 20% higher than that of the superheated model, however the results are still less than the experimental data. The increase of heat transfer in the results of this model was due to the increase of sensible heat transfer of the gas mixture near the interface.

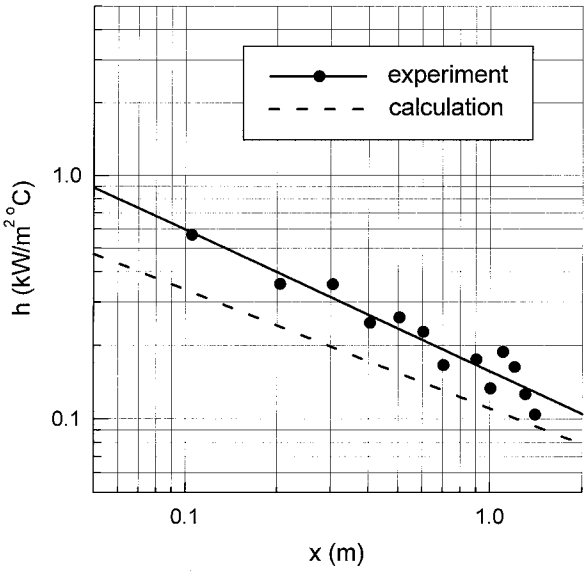

Fig. 10. Comparison of superheat model and experiment for local heat transfer coefficient of steam–air mixture having large temperature difference between bulk mixture and wall ($T_w = 22.5\ x^{-0.128}$°C (x unit in m), $T_{in} = 90°C$, $u_{in} = 2$ m/s, $\theta = 4.1°$, $x = 1.21$ m).

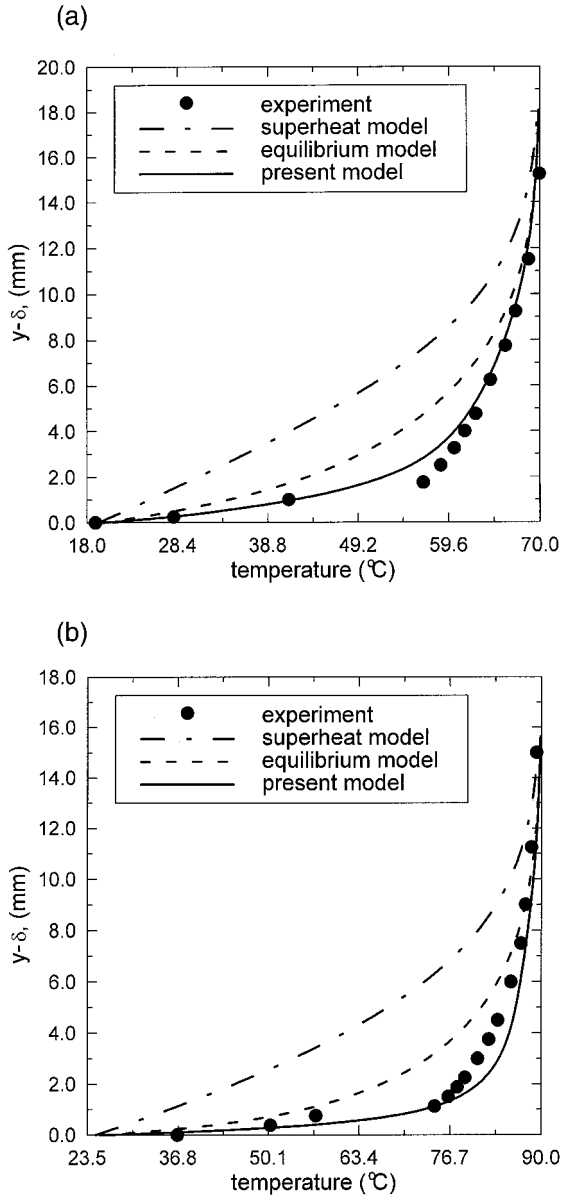

Fig. 11. Comparison of equilibrium and present models and experimental data for the temperature profiles of steam–air mixture having large temperature difference between bulk mixture and wall (case a: $T_w = 18.5°C$, $T_{in} = 70°C$, $u_{in} = 2$ m/s, $\theta = 4.1°$, $x = 1.21$ m; case b: $T_w = 23.7°C$, $T_{in} = 90°C$, $u_{in} = 2$ m/s, $\theta = 4.1°$, $x = 1.21$ m).

4.2.3. Present model

From the previous calculation and experimental results, we found that the bulk mixture in the boundary layer was supersaturated and had a higher temperature than the saturated temperature. It would be hard to assume that the steam–air mixture temperature is

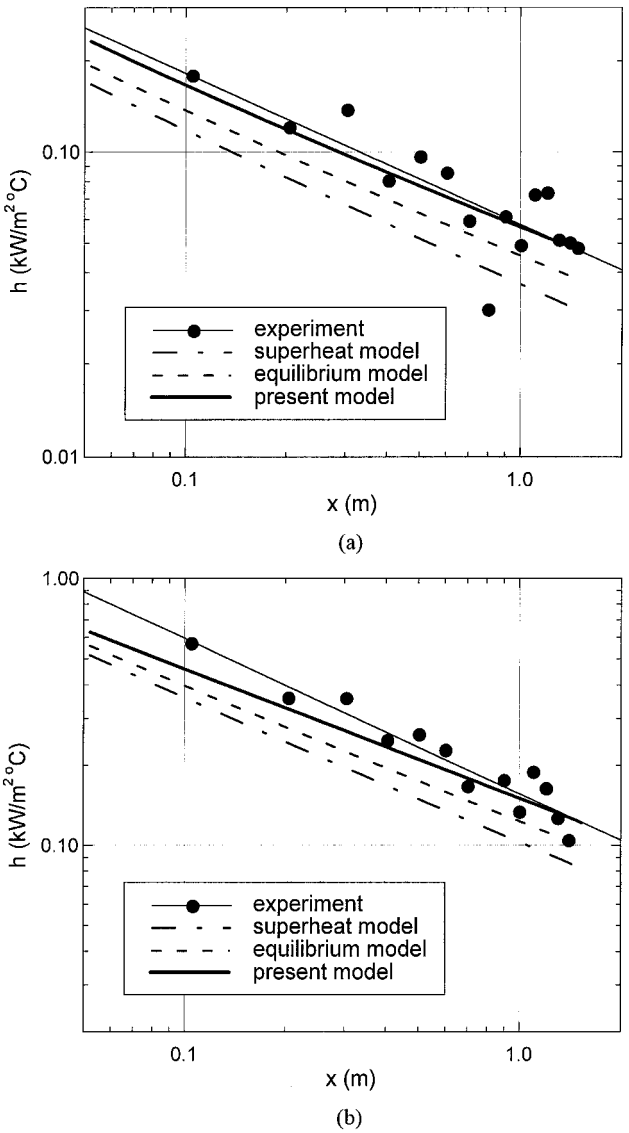

Fig. 12. Comparison of equilibrium and present models and experimental data for local heat transfer coefficient of steam–air mixture having large temperature difference between bulk mixture and wall (case a: $T_w = 19.1\ x^{-0.0661}$°C (x unit in m); case b: $T_w = 22.5\ x^{-0.128}$ °C (x unit in m), the other conditions are the same as Fig. 11).

superheated even though mist exists in the boundary layer. Droplets of mist in the boundary layer move toward the interface, since the bulk mixture flows toward the interface. Following the path, the mist is located at the more supersaturated condition except just above the interface as shown in Fig. 11. The mist will grow along the path. The mist temperature has higher temperature than that of the bulk mixture as discussed by Hill (1966) and Gyarmathy (1963). Therefore the bulk temperature of the mixture and the mist would be higher than the

saturated temperature. In this process, a higher mist temperature was expected at a higher degree of supersaturation. The present model simply assumed that some part of the latent heat is absorbed in the mist during this process and the portion is the ratio of P_{ssl}/P_{sat}.

The results are shown in Figs. 11 and 12. The ratios (P_{ssl}/P_{sat}) were 2.6 and 2.4 for the cases (a) and (b) in Figs. 11 and 12. The present model predicted well comparing the equilibrium and the superheated models. Conclusively, the heat transfer of supersaturated mixture is enhanced about several tens percents comparing the superheated mixture. The present model is only applicable in the present experimental range. More detailed study is needed to completely understand the characteristics of the condensation of supersaturated mixture.

5. Concluding remarks

Experiment and numerical simulations were conducted for the laminar film condensation of steam–air mixture flow over a flat plate. The temperature and velocity profiles were measured using the thermocouple and the LDA, and the heat transfer coefficients were measured and calculated for the saturated steam–air mixture. In the case of a small temperature difference between the saturated steam–air mixture and the cold wall, the gas mixture boundary layer can be treated as superheated gas. When the temperature difference was large, the gas mixtures become supersaturated near the interface. The gas mixture temperature profile was greatly concaved toward the interface, however the velocity profile was not. Enhancement of heat transfer was also found in this case. The superheated model without mist formation agreed well with the experimental data in the case of small temperature differences between saturated the steam–air mixture and the condensing wall. The equilibrium model, when the phase is changed at saturation conditions, underpredicted the heat transfer coefficient compared with the experimental data. The present model, in which some part of latent heat can be absorbed into the mist during the phase change, is proposed in this study. The model suggested showed the best agreement with the experimental results among three models. However more detailed study is needed to understand completely the characteristics of the condensation of supersaturated mixture.

Acknowledgements

This work was performed with financial support from the Center for Advanced Reactor Research.

References

Asano, K., Nakano, Y., Inaba, M., 1979. Forced convection film condensation of vapors in the presence of noncondensable gas on a small vertical plate. J. Chem. Engng Jap. 12, 196–202.

Brouwers, H.J.H., 1991. An improved tangency condition for fog formation in cooler-condensers. Int. J. Heat Mass Transfer 34, 2387–2394.

Brouwers, H.J.H., Chesters, A.K., 1992. Film models for transport phenomena with fog formation: the classical film model. Int. J. Heat Mass Transfer 35, 1–11.

Carey, V.P., 1992. Liquid–vapor phase-change phenomena. Hemisphere, Washington, DC, pp. 127–166.

Chen, S.L., Gerner, F.M., Tien, C.L., 1987. General film condensation correlations. Expl Heat Transfer 1, 93–107.

Corradini, M.L., 1984. Turbulent condensation on a cold wall in the presence of a noncondensable gas. Nucl. Technol. 64, 186–195.

Denny, V.E., Mills, A.F., Jusionis, V.J., 1971. Laminar film condensation from a steam–air mixture undergoing forced flow down a vertical surface. J. Heat Transfer 3, 297–304.

Desesquelles, F.L., Foch, B.P., 1986. Heat and mass transfer with condensation in laminar and turbulent boundary layers along a flat plate. Int. J. Heat Mass Transfer 29, 95–105.

Fox, R.J., Nagasaki, T., Hijikata, K., Peterson, P.F., 1993. Heat transfer and stability phenomena in gas loaded condensers. In: Proceedings of Sixth International Topical Meeting on Nuclear Reactor Thermal Hydraulics, France, vol. 2, pp. 1033–1041.

Gyarmathy, G., 1963. Kondensationsstoß-diagramme fur wasserdampfstromungen. Forsch. Ing.-Wes. 29, 106.

Hijikata, K., Mori, Y., 1973. Forced convective heat transfer of a gas with condensing vapour around a flat plate. Heat Transfer Jap. Res. 2, 81–101.

Hill, P.G., 1966. Condensation of water vapour during supersonic expansion in nozzles. J. Fluid Mech., Part 3 25, 593.

Jones, W.P., Renz, U., 1974. Condensation from a turbulent stream onto a vertical surface. Int. J. Heat Mass Transfer 17, 1019–1028.

Kang, H.C., Kim, M.H., 1994. Effect of noncondensable gas and wavy interface on the condensation heat transfer in a nearly horizontal plate. Nucl. Engng Des. 149, 313–321.

Kim, M.H., Corradini, M.L., 1990. Modelling of condensation heat transfer in a reactor containment. Nucl. Engng Des. 118, 193–212.

Kroger, D.G., Rohsenow, W.M., 1968. Condensation heat transfer in the presence of a non-condensable gas. Int. J. Heat Mass Transfer 11, 15–26.

Minkowycz, W.J., Sparrow, E.W., 1966. Condensation heat transfer in the presence of non-condensable, interfacial resistance, superheating, variable properties and diffusion. Int. J. Heat Mass Transfer 9, 1125–1144.

Mori, Y., Hijikata, K., 1973. Free convection condensation heat transfer with noncondensable gas on a vertical surface. Int. J. Heat Mass Transfer 16, 2229–2240.

Nusselt, W., 1916. Die Oberflähenkondensation des Wasserdampfes. Zeitschr. Veut. Ing. 60, 541–569.

Patanker, S.V., 1980. Numerical heat transfer and fluid flow. McGraw-Hill, New York.

Rauscher, J.W., Mills, A.F., Denny, V.E., 1974. Experimental study of film condensation from steam–air mixtures flowing downward over a horizontal tube. J. Heat Transfer 96, 83–88.

Reid, R.C., Prausnitz, J.M., Poling, B.E., 1986. The properties of gases and liquids, 4th ed. McGraw-Hill, New York, pp. 407–410.

Sparrow, E.M., Gregg, J.L., 1959. A boundary-layer treatment of laminar film condensation. J. Heat Transfer, Ser. C 83, 13–27.

Sparrow, E.W., Minkowycz, W.J., Saddy, M., 1967. Forced convection condensation in the presence of non-condensibles and interfacial resistance. Int. J. Heat Mass Transfer 10, 1829–1845.

Wylen, G.J.V., Sonntag, R.E., 1976. Fundamentals of classical thermodynamics, 2nd ed. Wiley, New York, pp. 555–558.

Wegener, P.P., Wu, B.J.C., 1977. Gas dynamics and homogeneous nucleation, advances in colloid and interface science. Elsevier, Oxford, pp. 325–417.